

Comparison of recent SnIa datasets

J. C. Bueno Sanchez^a, S. Nesseris^b and L. Perivolaropoulos^a

^a*Department of Physics, University of Ioannina, Greece*

^b*The Niels Bohr International Academy, The Niels Bohr Institute, Blegdamsvej 17, DK-2100, Copenhagen Ø, Denmark*

(Dated: October 28, 2018)

We rank the six latest Type Ia supernova (SnIa) datasets (Constitution (C), Union (U), ESSENCE (Davis) (E), Gold06 (G), SNLS 1yr (S) and SDSS-II (D)) in the context of the Chevalier-Polarski-Linder (CPL) parametrization $w(a) = w_0 + w_1(1 - a)$, according to their Figure of Merit (FoM), their consistency with the cosmological constant (Λ CDM), their consistency with standard rulers (Cosmic Microwave Background (CMB) and Baryon Acoustic Oscillations (BAO)) and their mutual consistency. We find a significant improvement of the FoM (defined as the inverse area of the 95.4% parameter contour) with the number of SnIa of these datasets ((C) highest FoM, (U), (G), (D), (E), (S) lowest FoM). Standard rulers (CMB+BAO) have a better FoM by about a factor of 3, compared to the highest FoM SnIa dataset (C). We also find that the ranking sequence based on consistency with Λ CDM is identical with the corresponding ranking based on consistency with standard rulers ((S) most consistent, (D), (C), (E), (U), (G) least consistent). The ranking sequence of the datasets however changes when we consider the consistency with an expansion history corresponding to evolving dark energy $(w_0, w_1) = (-1.4, 2)$ crossing the phantom divide line $w = -1$ (it is practically reversed to (G), (U), (E), (S), (D), (C)). The SALT2 and MLCS2k2 fitters are also compared and some peculiar features of the SDSS-II dataset when standardized with the MLCS2k2 fitter are pointed out. Finally, we construct a statistic to estimate the internal consistency of a collection of SnIa datasets. We find that even though there is good consistency among most samples taken from the above datasets, this consistency decreases significantly when the Gold06 (G) dataset is included in the sample.

PACS numbers: 98.80.Es, 98.65.Dx, 98.62.Sb

1. INTRODUCTION

The accelerating expansion of the universe has been indicated consistently by a wide range of cosmological data. The most sensitive probes of this expansion currently are standard candles in the form of Type Ia supernovae (SnIa) [1, 2, 3, 4, 5, 6, 7, 8, 9, 10] and standard rulers in the form of the sound horizon scale at last scattering as measured through the Cosmic Microwave Background (CMB) power spectrum [11, 12] and through Baryon Acoustic Oscillations (BAO) [13, 14, 15]. These cosmological observations have indicated [11, 12, 16, 17] that the simplest cosmological model consistent with the observed accelerating expansion is the Λ CDM model [18] (based on a cosmological constant) even though models based on dynamical dark energy [19] or modified gravity [20] remain viable alternatives.

Several new SnIa datasets have emerged during the last 3-4 years aiming at mapping in detail the accelerating expansion in the redshift range $z \in [0, 2]$. The main such datasets, analyzed in the present study, are shown in detail in Table 1 of the next section and include the compilations: Constitution [5], Union [6], ESSENCE [7], SNLS 1st year (SNLS1) [8], Gold06 [9] and SDSS-II [10]. As shown in Table 1 most of these compilations include subsets obtained with different instruments. Even though efforts have been made in most cases to reanalyze the SnIa light curves and reject outliers in order to smooth out potential systematics due to inhomogeneities of the samples, systematics remain as a source of uncertainties

[22, 23].

The above SnIa standard candle data (luminous sources of known intrinsic luminosity) are geometric probes used to measure the luminosity distance $d_L(z)$ which, assuming flatness, is connected to the Hubble expansion rate $H(z)$ as

$$d_L(z) = c(1+z) \int_0^z dz' \frac{1}{H(z')}, \quad (1.1)$$

where c is the velocity of light. Alternative geometric probes are standard rulers (objects of known comoving size). These may be used to measure the angular diameter distance $d_A(z)$ which, in a flat universe, is related to $H(z)$ as

$$d_A(z) = \frac{c}{1+z} \int_0^z dz' \frac{1}{H(z')}. \quad (1.2)$$

The most useful standard ruler in cosmology is the last scattering sound horizon ($z \simeq 1090$), the scale of which can be measured either directly through the CMB temperature power spectrum [11, 12, 24] or indirectly through Baryon Acoustic Oscillations (BAO) on the matter power spectrum at low redshifts [13, 14, 15]. These data lead to constraints on $H(z)$ that are independent from those of standard candles. Thus the mutual consistency of the standard candle and standard ruler constraints can be used as a quality test for both classes of data. This is one of the consistency tests implemented on SnIa datasets in the present study.

All of the above mentioned geometric probes aim at mapping the expansion rate $H(z)$ as a function of the redshift z . The determination of the Hubble parameter $H(z)$ is equivalent to identifying the function $w(z)$ defined as

$$w(z) = -1 + \frac{1}{3}(1+z) \cdot \frac{d \ln(H(z)^2/H_0^2 - \Omega_{0m}(1+z)^3 - \Omega_{0r}(1+z)^4)}{dz} \quad (1.3)$$

where the term in the logarithm accounts for all terms in the Friedmann equation not related to matter (present normalized density Ω_{0m}) and radiation (present normalized density Ω_{0r}). If the origin of the accelerating expansion is dark energy then $w(z)$ may be identified with the dark energy equation of state parameter $w(z) = \frac{p_x}{\rho_x}$. The cosmological constant ($w(z) = -1$) is the simplest dark energy model and corresponds to a constant dark energy density (Λ CDM model). The vast majority of presently available cosmological data are consistent with Λ CDM [17] at the 95.4% level (see however [25] and references therein for some puzzling exceptions).

In view of the increasing number of SnIa dataset compilations a need has emerged for ranking these compilations with respect to their Figure of Merit [26, 27] (FoM), defined as the inverse area of the 95% confidence region¹, their degree of consistency with Λ CDM, with standard candles and with each other. These consistency rankings require the derivation of suitable statistics designed to achieve them in an efficient manner. The goal of the present study is to provide such statistics and apply them in order to rank the SnIa compilations of Table 1 of section 2 according to

- their FoM in the context of the Chevalier-Polarski-Linder (CPL) [28], [29] parametrization of dynamical dark energy

$$w = w_0 + w_1(1-a) = w_0 + w_1 \frac{z}{1+z} \quad (1.4)$$

- their degree of consistency with Λ CDM
- their degree of consistency with standard ruler constraints of Ref. [12, 14] thus testing the quality of the SnIa data (assuming that the distance duality relation $d_L(z) = d_A(z)(1+z)^2$ is applicable)
- their degree of consistency with each other.

In the context of ranking the SnIa compilations with respect to their consistency with Λ CDM we make use of the CPL parametrization and assuming flatness, we identify the “distance” in units of σ (σ -distance $d_\sigma(\Omega_{0m})$) of the “reference” parameter space point $(w_0, w_1) = (-1, 0)$

corresponding to Λ CDM from the best fit point (w_0, w_1) of each SnIa dataset and for several priors of Ω_{0m} . Similarly, in order to rank the SnIa compilations with respect to their consistency with CMB-BAO standard rulers we follow the above method but we replace the Λ CDM “reference” point by the best fit $(w_0, w_1)^{SR}$ parameter values obtained in the context of standard ruler (CMB+BAO) data for each Ω_{0m} prior.

In addition to the σ -distance we also use the Binned Normalized Differences (BND) statistic of Ref. [30] to rank the datasets according to their consistency with Λ CDM. Finally, in the context of measuring the internal consistency of a set of n compilations we consider the mean σ -distance

$$\bar{d}_\sigma(\Omega_{0m}; w_0, w_1) \equiv \frac{1}{n} \sum_{i=1}^n d_{\sigma i}(\Omega_{0m}; w_0, w_1), \quad (1.5)$$

where $d_{\sigma i}(\Omega_{0m}; w_0, w_1)$ is the σ -distance from the reference parameter point (w_0, w_1) to the best fit point of the i^{th} compilation (see Fig. 7). Minimization of $\bar{d}_\sigma(\Omega_{0m}; w_0, w_1)$ at fixed Ω_{0m} leads to a minimum mean σ -distance and to the parameters (\bar{w}_0, \bar{w}_1) of maximum consistency for the particular set of compilations. Smaller $\bar{d}_\sigma(\Omega_{0m}; \bar{w}_0, \bar{w}_1)$ implies a better internal consistency for the set of compilations. Minimizing $\bar{d}_\sigma(\Omega_{0m}; \bar{w}_0, \bar{w}_1)$ with respect to Ω_{0m} we can also find the value of Ω_{0m} that maximizes the consistency among the SnIa data compilations.

The above statistics are applied on the SnIa data of Table 1 in the following sections. In section 2 we summarize the likelihood calculations needed to evaluate the σ -distances described above and briefly discuss the BND statistic described in detail in Ref. [30]. We also discuss the main features of the considered SnIa datasets and rank them according to their FoM. In section 3 we apply the σ -distance statistic and the BND statistic to rank the data of Table 1 according to their consistency with Λ CDM and with the CMB-BAO best fit. In section 4 we apply the mean σ -distance minimization to find the internal consistency of various sets of compilations obtained from Table 1. Finally in section 5 we conclude, summarize and discuss future prospects of the present study.

2. LIKELIHOOD ANALYSIS

Our likelihood analysis method is described in detail in Refs [31] and [32]. Here we only review some of the basic steps for completeness. We assume a CPL [28], [29] parametrization for $w(z)$ (equation (1.4)) and apply the maximum likelihood method separately for standard rulers (CMB+BAO) and standard candles (SnIa) assuming flatness. The corresponding late time form of $H(z)$ for the CPL parametrization is

$$H^2(z) = H_0^2[\Omega_{0m}(1+z)^3 + (1-\Omega_{0m})(1+z)^{3(1+w_0+w_1)} e^{\frac{-3w_1z}{(1+z)}}]. \quad (2.1)$$

¹ Note that we use the 2σ contour in parameter space instead of the 95% confidence region used by the Dark Energy Task Force.

In the context of constraints from standard rulers we use the datapoints $(R, l_a, 100\Omega_b h^2)$ of Ref. [12] (WMAP5) where R, l_a are two shift parameters [32].

For a flat prior, the 5-year WMAP data (WMAP5) measured best fit values are [12]

$$\bar{\mathbf{V}}_{\text{CMB}} = \begin{pmatrix} \bar{R} \\ \bar{l}_a \\ 100\Omega_b h^2 \end{pmatrix} = \begin{pmatrix} 1.710 \pm 0.019 \\ 302.10 \pm 0.86 \\ 2.2765 \pm 0.0596 \end{pmatrix} \quad (2.2)$$

The corresponding covariance matrix is [12]

$$\mathbf{C}_{\text{CMB}} = \begin{pmatrix} 0.000367364 & 0.00181498 & -0.000201759 \\ 0.00181498 & 0.731444 & -0.0315874 \\ -0.000201759 & -0.0315874 & 0.00355323 \end{pmatrix} \quad (2.3)$$

We thus define

$$\mathbf{X}_{\text{CMB}} = \begin{pmatrix} R - 1.710 \\ l_a - 302.10 \\ 100\Omega_b h^2 - 2.2765 \end{pmatrix} \quad (2.4)$$

and construct the contribution of CMB to the χ^2 as

$$\chi_{\text{CMB}}^2 = \mathbf{X}_{\text{CMB}}^T \mathbf{C}_{\text{CMB}}^{-1} \mathbf{X}_{\text{CMB}} \quad (2.5)$$

with the inverse covariance matrix

$$\mathbf{C}_{\text{CMB}}^{-1} = \begin{pmatrix} 2809.73 & -0.133381 & 158.356 \\ -0.133381 & 2.21908 & 19.7195 \\ 158.356 & 19.7195 & 465.728 \end{pmatrix} \quad (2.6)$$

Notice that χ_{CMB}^2 depends on the four parameters $(\Omega_m, \Omega_b, w_0$ and $w_1)$. In what follows we use the priors $h = 0.705$, $\Omega_b = 2.2765/100h^2$ [12].

In the case of BAO we also apply the maximum likelihood method [32] using the datapoints of Ref. [14] (SDSS5). For comparison, we have also considered the more recent data of Ref. [15] (SDSS7) and have found minor differences in the results (slightly reduced consistency with Λ CDM in the context of the CPL parametrization but no change in the ranking sequences). In some cases we show the results of both sets of datapoints (Figs. 3, 4a, 9a).

Following Ref. [32] we find the contribution of BAO to χ^2 as

$$\chi_{\text{BAO}}^2 = \mathbf{X}_{\text{BAO}}^T \mathbf{C}_{\text{BAO}}^{-1} \mathbf{X}_{\text{BAO}}. \quad (2.7)$$

The analysis of SnIa standard candles is also based on the method described in Ref. [32]. Two of the earliest and reliable datasets are the Gold06 dataset [9] and the Supernova Legacy Survey (SNLS) [8] dataset. The Gold06 dataset compiled by Riess et. al. is a set of supernova data from various sources analyzed in a consistent and robust manner with reduced calibration errors arising from systematics. It contains 152 points from previously published data plus 30 points with $z > 1$ discovered

by the HST[9]. Even though the Gold06 data are of high quality, they are plagued by non-uniformity (they are a collection of data obtained from various instruments) and they include a few outliers. Filtered versions of the Gold06 dataset attempting to deal with these problems have been included in subsequent compilations.

The SNLS is a 5-year survey of SnIa with $z < 1$. The SNLS has adopted a more efficient SnIa search strategy involving a ‘‘rolling search’’ mode where a given field is observed every third or fourth night using a single imaging instrument, thus reducing photometric systematic uncertainties. The published first year SNLS dataset (SNLS1) constitutes of 44 previously published nearby SnIa with $0.015 < z < 0.125$ plus 73 distant SnIa ($0.15 < z < 1$) discovered by SNLS, two of which are outliers and are not used in the analysis. At this point it should be mentioned that both SNLS and Gold06 are reliable datasets, however, the non-uniformity of the Gold06 makes it less reliable compared to SNLS which is significantly more uniform.

We will also use the ESSENCE SnIa dataset of Davis et. al. [7] which constitutes of four subsets: ESSENCE [33, 35] (60 points), SNLS1 [8] (57 points), nearby [4] (45 points) and HST [9] (30 points) and the Union SnIa dataset of Kowalski et. al. [6] which constitutes of 414 SnIa, reduced to 307 points after various selection cuts were applied in order to create a homogeneous and high-signal-to-noise dataset. Finally, we will also use the Constitution SnIa dataset of Hicken et. al. [5] which constitutes in total of 397 SnIa out of which 100 come from the new low- z CfA3 sample and the rest from the Union [6] dataset. The inclusion of the new low- z sample in the Constitution dataset is a major improvement over previous datasets because the previous sample of nearby SnIa was relatively small and based on early investigations, leading to significant systematic uncertainties. In our analysis we use the Constitution datasets analyzed with both SALT and MLCS17 fitters [5].

Finally, we also consider the recently released first year data of the SDSS-II [10] aiming to alleviate the lack of data at intermediate redshift. In our analysis we consider the largest combined sample of SnIa considered in [10]. This encompasses 103 SnIa from the SDSS-II, 33 nearby SnIa [34], 56 points from ESSENCE [35], 62 from SNLS [8] and 34 from HST [9] making up a total of 288 SnIa. Here, we consider the SDSS-II dataset analyzed with both the SALT2 light-curve fitter and the MLCS2k2 fitter[21] and we compare the corresponding consistencies with Λ CDM. We have made simple tests to ensure that our analysis agrees with the one from [10], but in the case of the SDSS-II dataset analyzed with the SALT2 fitter, there is some ambiguity as the authors of Ref. [10] have not released the necessary covariance matrix that accounts for the correlations between the shape luminosity parameter (x_1), the color parameter (c) and the overall flux normalization (x_0).

In Table 1 we give some details about the SnIa datasets used in this analysis, such as the redshift range or the

Table 1: The datasets used in the present analysis. See respective references for details on the sources of the SnIa data points.

Dataset	Date Released	Redshift Range	# of SnIa	Filtered subsets included	Refs
SNLS1	2005	$0.015 \leq z \leq 1.01$	115	SNLS [8], LR [1]	[8]
Gold06	2006	$0.024 \leq z \leq 1.76$	182	SNLS1 [8], HST [9], SCP [2], HZSST [3]	[9]
ESSENCE	2007	$0.016 \leq z \leq 1.76$	192	SNLS1 [8], HST [9], ESSENCE[35],[7]	[35],[7]
Union	2008	$0.015 \leq z \leq 1.55$	307	Gold06 [9], ESSENCE[35],[7]	[6]
Constitution	2009	$0.015 \leq z \leq 1.55$	397	Union [6], CfA3[5]	[5]
SDSS	2009	$0.022 \leq z \leq 1.55$	288	Nearby [34], SDSS-II [10], ESSENCE [35], SNLS [8], HST [9]	[10]

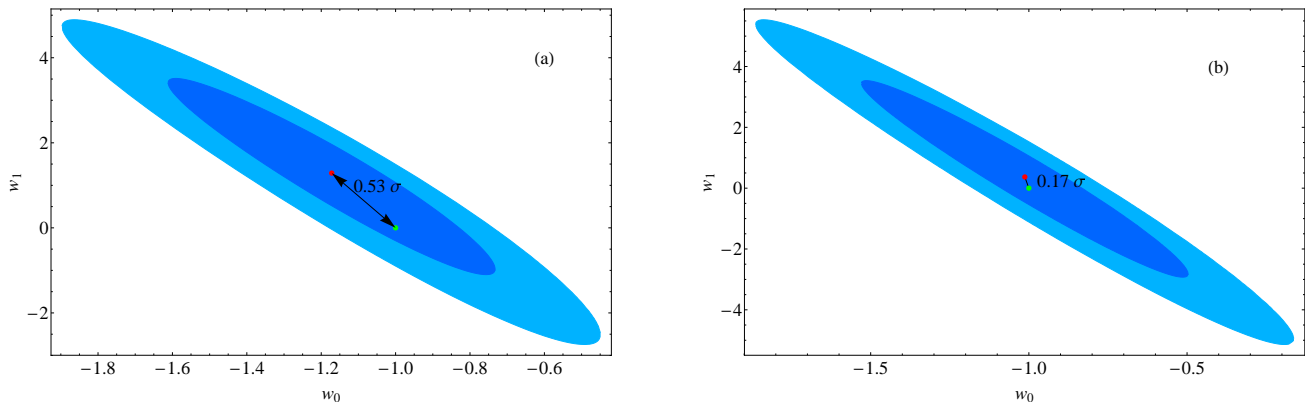


Fig. 1: The 68.3%(1 σ) – 95.4% (2 σ) χ^2 confidence contours in the $w_0 - w_1$ plane based on parametrization (2.1) for the ESSENCE (left) and SNLS1 datasets (right) for $\Omega_{0m} = 0.24$. The arrows indicate the σ -distance of Λ CDM (green points: $(w_0, w_1) = (-1, 0)$) to the best fit points (red points).

subsets of each set.

The SnIa observations use proper light curve fitters[21] to provide the apparent magnitude $m(z)$ of the supernovae at peak brightness. The resulting apparent magnitude $m(z)$ is related to the dimensionless luminosity distance $D_L(z)$ through

$$m_{th}(z) = \bar{M}(M, H_0) + 5\log_{10}(D_L(z)), \quad (2.8)$$

where we have used the notation of Ref. [32]. The theoretical model parameters are determined by minimizing the quantity

$$\chi_{SnIa}^2(\Omega_m, w_0, w_1) = \sum_{i=1}^N \frac{(\mu_{obs}(z_i) - \mu_{th}(z_i))^2}{\sigma_{\mu i}^2} \quad (2.9)$$

where N is the number of SnIa of the dataset and $\sigma_{\mu i}^2$ are the errors due to flux uncertainties, intrinsic dispersion of SnIa absolute magnitude and peculiar velocity dispersion. These errors are assumed to be Gaussian and uncorrelated. The theoretical distance modulus is defined as

$$\mu_{th}(z_i) \equiv m_{th}(z_i) - M = 5\log_{10}(D_L(z)) + \mu_0, \quad (2.10)$$

where

$$\mu_0 = 42.38 - 5\log_{10}h, \quad (2.11)$$

The steps we followed for the usual minimization of (2.9) in terms of its parameters are described in detail in Refs. [31, 36, 37].

In order to study the consistency of the various SnIa datasets with the cosmological constant and the standard rulers we consider the distance in units of σ (σ -distance d_σ) of the best fit point to a model with parameters (w_0, w_1) , where this reference point can be either Λ CDM or some other reference point, (see Fig. 1). The σ -distance can be found by converting $\Delta\chi^2 = \chi_{(w_0, w_1)}^2 - \chi_{min}^2$ to d_σ , i.e. solving [38]

$$1 - \Gamma(1, \Delta\chi^2/2)/\Gamma(1) = \text{Erf}(d_\sigma/\sqrt{2}) \quad (2.12)$$

for d_σ (σ -distance), where $\Delta\chi^2$ is the χ^2 difference between the best-fit and the reference point (w_0, w_1) (eg Λ CDM) and $\text{Erf}()$ is the error function. The right hand side of Eq. (2.12) comes from integrating $\int_{-n\sigma}^{n\sigma} \frac{1}{\sigma\sqrt{2\pi}} e^{-\frac{x^2}{2\sigma^2}} dx$, where n is the desired number of

Table 2: The Figure of Merit (FoM) for the datasets of Table 1 for $\Omega_{0m} = 0.28$ using the CPL parametrization. For comparison we also show the corresponding FoM obtained with standard ruler data.

Dataset	# of SnIa	Figure of Merit
SNLS1	115	0.208
Gold06	182	0.367
ESSENCE	192	0.245
SDSS-II (SALT2)	288	0.366
SDSS-II (MLCS2k2)	288	0.553
Union	307	0.512
Constitution (SALT2)	397	0.708
CMB+SDSS5	-	2.028
CMB+SDSS7	-	2.541

σ s, while the left hand side corresponds to the Cumulative Distribution Function (CDF) of a χ^2 distribution [38] with two degrees of freedom. Note that Eq. (2.12) is only valid for the two parameters (w_0, w_1) and should be generalized accordingly for more parameters [38]. In the special case of $n = 1$ or $n = 2$ we obtain the well known results $\Delta\chi_{1\sigma} = 2.30$ and $\Delta\chi_{2\sigma} = 6.18$ valid for two parameter parametrizations [38].

Even though the σ -distance is not a commonly used statistic it is quite useful because it can directly give information about probability of a given region in parameter space. The integer values of sigma distance (1σ and 2σ) are commonly used to draw the corresponding contours in parameter space. We have extended this statistic to non-integer values in order to find the specific contours that go through particular reference points of parameter space and thus estimate quantitatively the consistency of these points. The advantage of using the σ -distance instead of $\Delta\chi^2$ is the fact that the σ -distance takes into account the number of parameters of the parameterizations and can therefore be directly translated into probability for each point in parameter space. This is not possible for $\Delta\chi^2$ because it does not include information about the number of parameters of the parameterizations considered.

The Figure of Merit (FoM) is a useful measure of the effectiveness of a set of data in constraining cosmological parameters. In the case of two parameters (as for the CPL parametrization) it is defined as the reciprocal area of the 95.4% contour, in parameter space (w_0, w_1) [26, 27]. Clearly, the larger the FoM the more effective the dataset in constraining the parameters (w_0, w_1) . In Table 2 we show the FoM for each dataset of Table 1 for a prior of $\Omega_{0m} = 0.28$. In Fig. 2 we show the FoM in terms of the

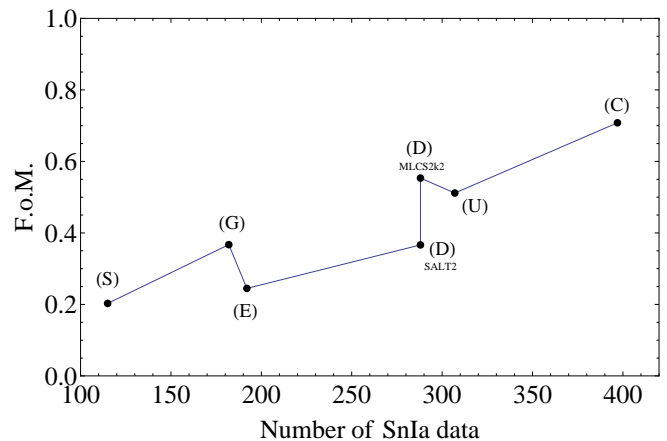


Fig. 2: The Figure of Merit (FoM) in terms of the number of the SnIa data for $\Omega_{0m} = 0.28$ using the CPL parametrization.

number of the SnIa data for the same datasets. Clearly, the FoM is an increasing function of the number of SnIa in the datasets. An exception to this rule is the ESSENCE dataset which has a slightly smaller FoM compared to the Gold06 dataset even though it has a larger number of SnIa.

We should stress that the FoM does not depend only on the total number of SnIa of the dataset but mainly on the number of SnIa at low and high redshifts. This sensitivity on the distribution in redshift space is most probably the origin of the ESSENCE glitch in the FoM plot of Fig. 2. Notice that the redshift space distribution of the ESSENCE data includes more data at intermediate redshifts than the Gold06 dataset while the number of SnIa in the ESSENCE dataset is similar to that of the Gold06 dataset. Finally, for comparison, in the same table we show the FoM corresponding to standard ruler data (WMAP5+SDSS5 and WMAP5+SDSS7). Clearly, the FoM of standard rulers is about a factor of 3 higher compared to the highest FoM of SnIa corresponding to the Constitution dataset.

In addition to using d_σ to rank SnIa datasets, we consider the BND statistic [30] which is designed to pick up systematic brightness trends of SnIa datapoints with respect to a best fit cosmological model at high redshifts. It is based on binning (considering the average of) the normalized differences between the SnIa distance moduli and the corresponding best fit values in the context of a specific cosmological model (e.g. Λ CDM). These differences are normalized by the standard errors of the observed distance moduli (BND). As in Ref. [30] we will focus on the highest redshift bin and extend its size towards lower redshifts until the BND changes sign (crosses 0) at a redshift z_c (bin size N_c). The bin size N_c of this crossing (the statistical variable) is then compared with the corresponding crossing bin size N_{mc} for Monte Carlo data realizations based on the best fit model.

In Ref. [30] it was found that the crossing bin size N_c obtained from the Union and Gold06 data with respect to

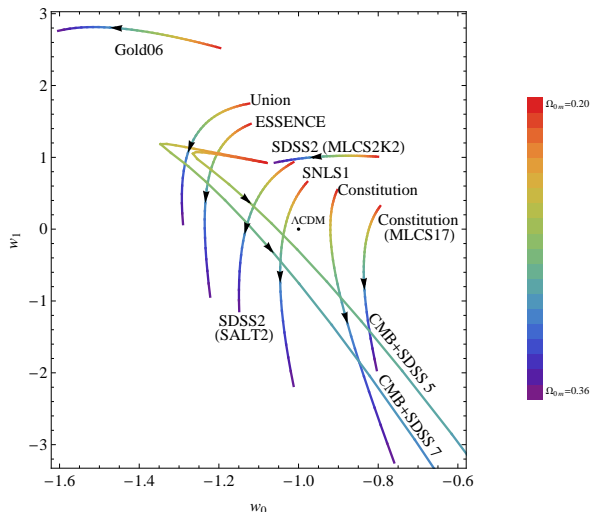


Fig. 3: Trajectories of the best fit points (w_0, w_1) obtained for each of the datasets of Table 1 and also for the standard ruler CMB-BAO (WMAP5+SDSS5 and WMAP5+SDSS7) data as Ω_{0m} varies in the range $\Omega_{0m} \in [0.2, 0.36]$. The arrows in the best fit lines indicate the direction of growing Ω_{0m} . Note that for the SDSS5 data the standard ruler best fit parameters stretch out to $(w_0, w_1) \simeq (2, -30)$ for $\Omega_{0m} \simeq 0.36$, whereas for the SDSS7 data $(w_0, w_1) \simeq (0.90, -20)$.

the best fit Λ CDM model is anomalously large compared to N_{mc} of the corresponding Monte Carlo datasets obtained from the best fit Λ CDM in each case. In the next section we will extend this analysis to all the datasets of Table 1 and use the results to rank these datasets according to their consistency with Λ CDM.

3. CONSISTENCY OF DATASETS WITH Λ CDM AND WITH STANDARD RULERS

It is straightforward to apply the likelihood methods described in the previous section to find the trajectory of the best fit point (w_0, w_1) in parameter space as Ω_{0m} varies in the range $\Omega_{0m} \in [0.2, 0.36]$. These trajectories obtained for each of the datasets of Table 1 and also for the standard ruler CMB-BAO (WMAP5+SDSS5, WMAP5+SDSS7) data are shown in Fig. 3. These trajectories can not be used to directly rank the datasets according to their consistency with any given reference point in parameter space (e.g. Λ CDM) because they contain no information about the 68.3% contours (the plot would become confusing if we attempted to include such contours). However, they provide useful hints for the trend of the best fit parameters as Ω_{0m} varies. For example, such a trend is the increase of the best fit value of the slope w_1 as the prior of Ω_{0m} decreases towards the value 0.2 or that the best fit value of w_0 remains less than -1 for all datasets except of the Constitution

Dataset	d_σ^{min}	Ω_{0m}^{min}	w_0	w_1
SNLS1	0.004	0.260	-1.03	0.16
SDSS-II (SALT2)	0.084	0.270	-1.09	0.51
Constitution	0.114	0.285	-0.91	-0.54
ESSENCE	0.227	0.270	-1.20	1.04
Union	0.525	0.285	-1.25	1.40
SDSS-II (MLCS2K2)	0.623	0.360	-1.06	0.93
Gold06	0.950	0.345	-1.56	2.80
CMB+BAO (SDSS5)	0.200	0.272	-1.15	0.51
CMB+BAO (SDSS7)	0.588	0.272	-1.30	0.97

Table 3: Minimum σ -distance $d_\sigma^{min}(\Omega_{0m}^{min}; -1, 0)$ from the best fit point for each of the datasets to the Λ CDM point. Also listed are the corresponding values of Ω_{0m} , and the best fit parameters (w_0, w_1) (see also Fig. 4a). The SDSS-II (MLCS2K2) data showed no minimum of d_σ with respect to Ω_{0m} in the range $\Omega_{0m} \in [0.2, 0.36]$. We thus have simply displayed the lowest value of d_σ in the corresponding range of Ω_{0m} .

compilation.

The ranking sequence of the datasets of Table 1 with respect to any reference point in parameter space can be studied quantitatively using the σ -distance statistic discussed above. In order to test the sensitivity of the ranking sequence of datasets with respect to the choice of consistency reference point (w_0, w_1) we consider two such reference points: $(w_0, w_1) = (-1, 0)$ (Λ CDM) and $(w_0, w_1) = (-1.4, 2)$ which corresponds to dynamical dark energy with a $w(z)$ that crosses the line $w = -1$. It should be noted that there is nothing special about the parameter point $(-1.4, 2)$. We have selected it as a representative of a wide region in parameter space (upper left from Λ CDM) which corresponds to dynamical dark energy crossing the phantom divide line $w = -1$. Any other point in the same parameter region would lead to similar results and the same ranking of datasets. This particular parameter region is interesting because it is spanned by the best fit trajectories and it also mildly favored by the Gold06 dataset (see Fig. 3).

The resulting $d_\sigma(\Omega_{0m})$ for each dataset of Table 1 are shown in Figs. 4a and 4b in the range $\Omega_{0m} \in [0.2, 0.36]$. Clearly, there are values of Ω_{0m} that minimize the σ -distance $d_\sigma(\Omega_{0m})$ between the best fit of each dataset and the reference point. These values of Ω_{0m} maximize the consistency of the datasets with the given reference point in this range of Ω_{0m} . The minima σ -distances $d_\sigma(\Omega_{0m})$ for each dataset, corresponding to maximum consistency with Λ CDM along with the corresponding values of Ω_{0m} are shown (properly ranked) in Table 3. The corresponding results for the reference point $(w_0, w_1) = (-1.4, 2)$ are shown in Table 4.

The following comments can be made with respect to the results shown in Figs. 4a, 4b and in the corresponding Tables 3, 4.

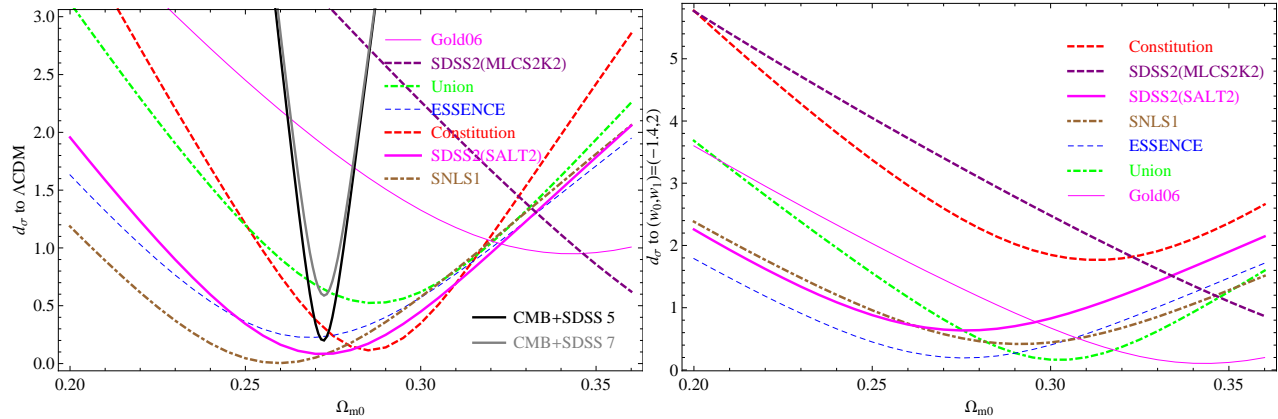


Fig. 4: a: σ -distances $d_{\sigma_i}(\Omega_{0m}; -1, 0)$ off the Λ CDM point (reference point) from the best fit of each dataset in Table 1. Notice that they are minimized at similar values of Ω_{0m} . The σ -distance $d_{\sigma}(\Omega_{0m}; -1, 0)$ between the standard ruler best fits and Λ CDM are also shown as a function of Ω_{0m} (black and grey solid lines). b: Similar to (a) for the dynamical dark energy reference point $(w_0, w_1) = (-1.4, 2)$. Notice that the σ -distances $d_{\sigma_i}(\Omega_{0m}; -1.4, 2)$ are minimized at more widely separated values of Ω_{0m} .

Dataset	d_{σ}^{min}	Ω_{0m}^{min}	w_0	w_1
Gold06	0.11	0.345	-1.56	2.80
Union	0.17	0.300	-1.26	1.25
ESSENCE	0.19	0.275	-1.21	0.99
SNLS1	0.42	0.290	-1.04	-0.26
SDSS-II (SALT2)	0.63	0.275	-1.10	0.46
SDSS-II (MLCS2K2)	0.87	0.360	-1.06	0.93
Constitution	1.77	0.315	-0.88	-1.32

Table 4: The minimum σ -distances d_{σ}^{min} to the reference point $(w_0, w_1) = (-1.4, 2)$, the values of Ω_{0m} at which the minimum distance is attained, and the best fit parameters (w_0, w_1) at Ω_{0m}^{min} are displayed for each dataset (see also Fig. 4b). We omit the rows corresponding to CMB+BAO data as the resulting σ -distance is always $\gg 1$ due to the dominance of the dark energy at early times. The SDSS-II (MLCS2K2) data showed no minimum of d_{σ} with respect to Ω_{0m} in the range $\Omega_{0m} \in [0.2, 0.36]$. We thus have simply displayed the lowest value of d_{σ} in the corresponding range of Ω_{0m} .

1. The consistency with Λ CDM of all datasets, except Gold06 and SDSS-II when using the MLCS2K2 method, is maximized in a narrow range of $\Omega_{0m} \in [0.26, 0.29]$ which also includes the value of Ω_{0m} favored by standard rulers. On the other hand, the consistency with the dynamical dark energy point $(w_0, w_1) = (-1.4, 2)$ is maximized over a wider range of Ω_{0m} ($\Omega_{0m} \in [0.27, 0.35]$) thus decreasing the consistency among the datasets in the context of dynamical dark energy.
2. The ranking sequence changes dramatically when the consistency with the dynamical dark energy is considered as a reference point instead of Λ CDM

Dataset	Prob. of Consistency	Best Fit Ω_{0m}
SNLS1	79%	0.26
SDSS2-SALT2	68%	0.28
SDSS2-MLCS2k2	52%	0.40
ESSENCE	30.4%	0.27
Constitution	12.6 %	0.29
Union	5.3 %	0.29
Gold06	2.5%	0.34

Table 5: Consistency of SNIa datasets with Λ CDM according to the BND statistic. Notice the high Ω_{0m} value favored by the SDSS2-MLCS2k2 dataset which is a few σ above the value favored by other observations.

(Table 4). Essentially the ranking is reversed! Thus, the choice of the consistency reference point plays an important role in determining the ranking sequence of the datasets (see also Fig. 3).

3. The SDSS-II dataset obtained with the MLCS2k2 fitter has some peculiar features compared to other datasets. In particular it favors particularly high values of Ω_{0m} ($\Omega_{0m} \simeq 0.4$) while for $\Omega_{0m} < 0.3$ its consistency with Λ CDM is significantly reduced to a level of 3σ or larger ($d_{\sigma} > 3$). In addition, the trajectory of its best fit parameter point as Ω_{0m} varies is perpendicular to the corresponding trajectory of most other datasets (see Fig. 3).

An alternative ranking of the SNIa datasets according to their consistency with Λ CDM can be made using the BND statistic described briefly in section 2 and in more detail in Ref. [30]. When applying the BND statistic to find the consistency of a given dataset with Λ CDM, we find the fraction of Monte Carlo datasets (generated from

Dataset	d_{σ}^{min}	Ω_{0m}^{min}	w_0	w_1	w_0^{SR}	w_1^{SR}
SNLS1	0.003	0.280	-1.04	-0.10	-1.07	0.08
SDSS-II (SALT2)	0.058	0.280	-1.11	0.40	-1.07	0.08
ESSENCE	0.087	0.275	-1.21	0.99	-1.12	0.38
Constitution	0.121	0.295	-0.90	-0.76	-0.84	-1.28
Union	0.681	0.280	-1.24	1.44	-1.07	0.08
Gold06	1.976	0.280	-1.38	2.75	-1.07	0.08
SDSS-II(MLCS2K2)	3.342	0.285	-0.92	1.02	-1.00	-0.28

Table 6: Consistency with standard rulers. Minimum σ -distance $d_{\sigma i}^{min}(\Omega_{0m}; (w_0, w_1)^{SR})$ between best fit parameters for each dataset, (w_0, w_1) , and best fit for standard rulers, $(w_0, w_1)^{SR}$. $d_{\sigma i}^{min}(\Omega_{0m}; (w_0, w_1)^{SR})$ is minimized at Ω_{0m}^{min} (see Fig. 6).

the best fit Λ CDM model) that can mimic a BND crossing redshift z_c (or crossing bin-size N_c) similar to that of the real data. These Monte-Carlo datasets have $z_{mc} \leq z_c$ (or equivalently $N_{mc} \geq N_c$) and their fraction represents a probability of consistency of the given dataset with the model used to generate the Monte-Carlo datasets (best fit Λ CDM).

An example of a distribution of crossing bin sizes N_{mc} of such Monte-Carlo datasets is shown in Fig. 5 for the case of the Constitution dataset. In this case the best fit Λ CDM model has $\Omega_{0m} = 0.29$ and it is used to generate 222 Monte-Carlo realizations of the Constitution dataset as described in Ref. [30]. The distribution of the crossing bin sizes N_{mc} of these datasets are shown in Fig. 5 along with the crossing bin size of the real Constitution data (thick dashed green line). In this case, the probability of consistency of the Constitution dataset with the Monte Carlo data of Λ CDM ($N_{mc} > N_c$) is 12.6%.

Repeating the same process for all six datasets of Table 1 we assign to each of them a probability of consistency with Λ CDM which is shown in Table 5. Notice that the ranking sequence of consistency with Λ CDM obtained with the BND statistic is practically equivalent with the corresponding ranking obtained with the σ -distance statistic. This is reassuring for both ranking approaches.

It is straightforward to apply the σ -distance statistic to rank the SNIa datasets according to their consistency with standard ruler CMB-BAO data. We simply use as a consistency reference point the best fit point $(w_0, w_1)^{SR}$ for standard rulers obtained as described in section 2 using the WMAP5+SDSS5 data. In this case, the location of the reference point $(w_0, w_1)^{SR}$ in parameter space depends on Ω_{0m} but this does not complicate the analysis. The σ -distance between the reference point $(w_0, w_1)^{SR}$ and the best fit of each dataset is shown in Fig. 6 as a function of Ω_{0m} for the datasets of Table 1. These distances are minimized for values of Ω_{0m} that are different for each dataset but they are all in the narrow range $\Omega_{0m} \in [0.27, 0.3]$.

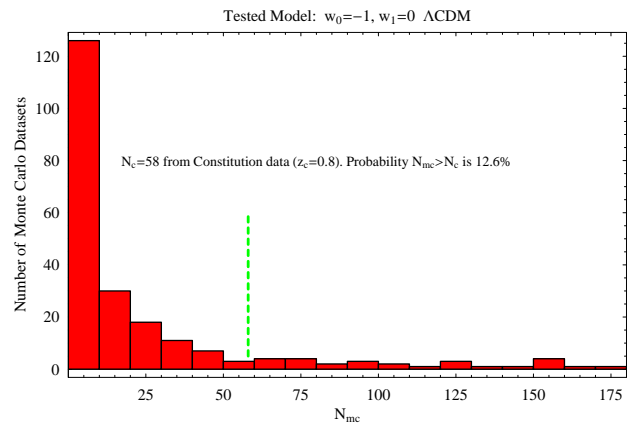


Fig. 5: The distribution of the crossing bin sizes N_{mc} of 222 Monte-Carlo datasets along with the crossing bin size of the real Constitution data (thick dashed green line).

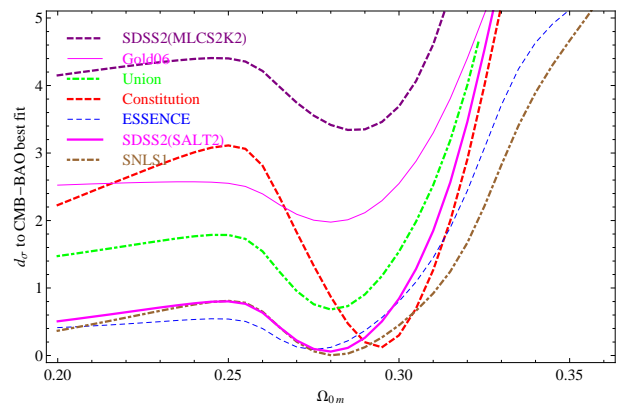


Fig. 6: σ -distance $d_{\sigma i}(\Omega_{0m}; (w_0, w_1)^{SR})$ between the reference point $(w_0, w_1)^{SR}$ of standard rulers (using the WMAP5+SDSS5 data) and the best fit of each dataset as a function of Ω_{0m} for the datasets of Table 1. Using the SDSS7 data, the minimum distances are found in the range $\Omega_{0m} \in [0.29, 0.31]$.

These minimum distances along with the corresponding value of Ω_{0m} are shown in Table 6 for each dataset (properly ranked according to consistency with standard rulers). Notice that the ranking sequence for the consistency with standard rulers is practically identical to the ranking sequence of the consistency with Λ CDM (Table 3) but differs from the ranking sequence of the consistency with dynamical dark energy (Table 4). This is an interesting feature of the data in favor of Λ CDM.

Using the SDSS7 data the distance to the standard rulers best fit for each dataset we find the minima shifted at slightly larger values of Ω_{0m} . We find that all of the minima lie in the range $\Omega_{0m} \in [0.29, 0.31]$ whereas the ranking sequence of Table 6 is maintained.

As shown in Fig. 6 the SDSS-II dataset obtained with the MLCS2k2 fitter has reduced consistency not only

Collection	$\langle \bar{d}_\sigma^{min} \rangle$	Var \bar{d}_σ^{min}
ES	0.03	0.0010
CS	0.13	0.0001
CES	0.20	0.0003
CE	0.21	0.0022
CUES	0.26	0.0043
CUS	0.28	0.0093
CUE	0.29	0.0147
CU	0.31	0.0392
SG	0.45	0.0194
CUESG	0.47	0.0163

Table 7: Table of internal consistency of dataset collections. The different datasets are labelled by C (Constitution), U (Union), E (ESSENCE), S (SNLS1), and G (Gold06). $\langle \bar{d}_\sigma^{min} \rangle$ and Var \bar{d}_σ^{min} stand for the average \bar{d}_σ^{min} over the range $\Omega_{0m} \in [0.20, 0.36]$ and its variance, respectively.

Collection	\bar{d}_σ^{min}	Ω_{0m}^{min}
ES	0.12	0.265
CS	0.16	0.280
CES	0.20	0.275
CE	0.21	0.280
CUES	0.29	0.280
CUS	0.29	0.280
CU	0.32	0.285
CUE	0.32	0.285
CUESG	0.57	0.285
SG	0.93	0.290

Table 8: Minimum mean σ -distance $\bar{d}_\sigma^{min}(\Omega_{0m}^{min}; -1, 0)$ from the best fit parameters of various dataset collections, to the Λ CDM parameter point.

with Λ CDM (as noted above) but also with standard rulers. Its distance from the standard ruler best fit is at the level of $3-4\sigma$ ($d_\sigma \simeq 3-4$). This is an additional indication of the peculiar nature of this dataset. In contrast the SDSS-II dataset obtained with the SALT2 fitter appears normal and consistent with Λ CDM, standard ruler and with the rest of the datasets (see Fig. 3).²

² In an effort to test the validity of our analysis for the SDSS-II datasets we have reproduced successfully the χ^2 contours of Ref. [10] (Figs. 26e and 35e) in the simplified constant w parametrization considered there. Note that following Ref. [10] we have only considered statistical errors.

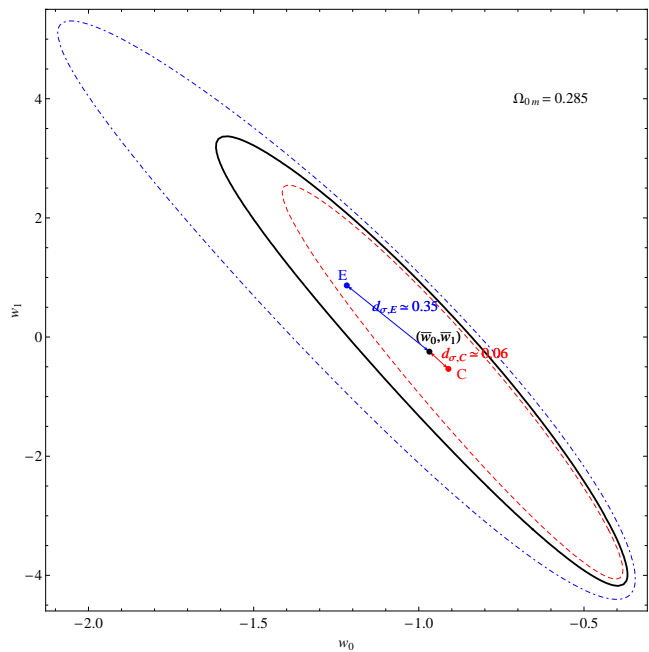


Fig. 7: Construction of $\bar{d}_\sigma(\Omega_{0m}; w_0, w_1)$ for a given point (w_0, w_1) in parameter space. The σ -distance between the reference point and the best fit of each SnIa dataset in a particular collection is evaluated using likelihood methods and then the mean σ -distance is obtained using Eq. (1.5). The figure illustrates the point (\bar{w}_0, \bar{w}_1) where the mean σ -distance \bar{d}_σ (obtained by collecting the Constitution and ESSENCE datasets) attains its minimum for a prior $\Omega_{0m} = 0.285$. The points E and C represent the best fit parameters for the Constitution and ESSENCE datasets. Also in the figure we show the 95.4% contours for the Constitution (dashed) and ESSENCE (dot-dashed) datasets, and the contour $\bar{d}_\sigma(\Omega_{0m}; w_0, w_1) = 2$ (thick, solid line).

4. INTERNAL CONSISTENCY OF SNIa DATASET COLLECTIONS

In this section we test the internal consistency of various collections of SnIa datasets using the mean σ -distance statistic $\bar{d}_\sigma(\Omega_{0m}; w_0, w_1)$ defined by Eq. (1.5). In Fig. 7 we show an example demonstrating the construction of $\bar{d}_\sigma(\Omega_{0m}; w_0, w_1)$ for a given point (w_0, w_1) in parameter space.

We minimize $\bar{d}_\sigma(\Omega_{0m}; w_0, w_1)$ with respect to (w_0, w_1) and find the parameter point (\bar{w}_0, \bar{w}_1) of maximum consistency with the given dataset collection as well as the minimum mean σ -distance $\bar{d}_\sigma^{min}(\Omega_{0m}; \bar{w}_0, \bar{w}_1)$ indicating the level of consistency. This minimized distance is shown in Fig. 8 as a function of Ω_{0m} for various dataset collections. Clearly, $\bar{d}_\sigma^{min}(\Omega_{0m}; \bar{w}_0, \bar{w}_1)$ is weakly dependent on Ω_{0m} but depends sensitively on the dataset collection considered.

Marginalizing $\bar{d}_\sigma^{min}(\Omega_{0m}; \bar{w}_0, \bar{w}_1)$ with respect to Ω_{0m} in the range $\Omega_{0m} \in [0.2, 0.36]$ we find $\langle \bar{d}_\sigma^{min} \rangle$ and its variance which may be directly used as a measure of the internal consistency of a given dataset collection.

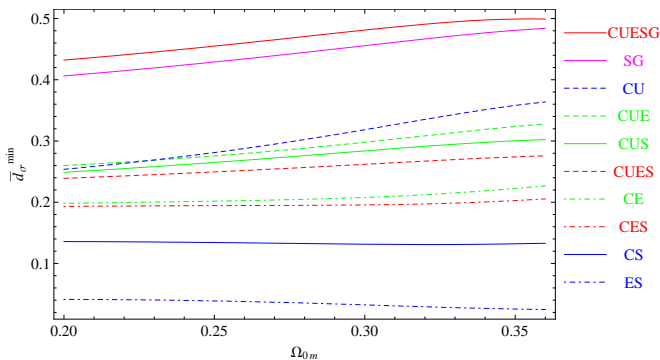


Fig. 8: Minimum mean σ -distance $\bar{d}_\sigma^{\min}(\Omega_{0m}; w_0, w_1)$ for the dataset collections considered in Table 7. The sequence of the legend corresponds to the sequence of lines in the plot.

To summarize, the derivation and use of our statistic involves the following steps:

1. Minimize the mean σ -distance defined by Eq. (1.5), with respect to (w_0, w_1) .
2. Marginalize the resulting minimum mean σ -distance over Ω_{0m} . This step is not important due to the weak dependence of the minimum σ -distance on Ω_{0m} (see Fig. 8). The evaluation of the (small) variance with respect to Ω_{0m} is only used to demonstrate the weak dependence of the mean σ -distance on Ω_{0m} and plays no further role in the analysis.
3. Use the marginalized (over Ω_{0m}) minimum (with respect to (w_0, w_1)) mean σ -distance as a measure of the internal consistency of the dataset collection. The smaller the minimum mean σ -distance is, the 'closer' together are the best fit parameter values in parameter space.

The values of $\langle \bar{d}_\sigma^{\min} \rangle$ and their variances for various dataset collections (properly ranked) are shown in Table 7. The following comments can be made with respect to the results shown in Table 7:

- All dataset collections considered are mutually consistent in the sense that the mean σ -distance between the best fits of each dataset and the point of maximum consistency is less than 1 (1σ).
- Collections including the Gold06 dataset have significantly less internal consistency than other dataset collections.
- Maximum internal consistency is achieved for the ESSENCE-SNLS1 collection ($\langle d_\sigma \rangle = 0.03$) and for the Constitution-SNLS1 collection ($\langle d_\sigma \rangle = 0.13$) which are collections that also maximize consistency with Λ CDM and CMB-BAO standard rulers (see below).

Collection	\bar{d}_σ^{\min}	Ω_{0m}^{\min}	w_0^{SR}	w_1^{SR}
ES	0.06	0.280	-1.07	0.08
CS	0.16	0.290	-0.93	-0.73
CES	0.23	0.290	-0.93	-0.73
CE	0.28	0.290	-0.93	-0.73
CUES	0.36	0.285	-1.00	-0.28
CUS	0.41	0.290	-0.93	-0.73
CUE	0.48	0.285	-1.00	-0.28
CU	0.55	0.290	-0.93	-0.73
CUESG	0.69	0.285	-1.00	-0.28
SG	0.99	0.280	-1.07	0.08

Table 9: Minimum mean σ -distance $\bar{d}_\sigma^{\min}(\Omega_{0m}^{\min}; (w_0, w_1)^{SR})$ from the best fit parameters of each dataset in a particular collection to the standard ruler best fit parameters $(w_0, w_1)^{SR}$.

In order to rank the consistency of *collections* of datasets with Λ CDM and with standard rulers we consider the mean σ -distances from Λ CDM $\bar{d}_\sigma(\Omega_{0m}; -1, 0)$ and from the standard ruler best fit $\bar{d}_\sigma(\Omega_{0m}; w_0^{SR}, w_1^{SR})$ (for the standard ruler best fit (w_0^{SR}, w_1^{SR})). These are shown in Fig. 9 as functions of Ω_{0m} . We then minimize these distances with respect to Ω_{0m} and find the corresponding \bar{d}_σ^{\min} distances. These may now be used to rank the dataset collections with respect to their consistency with either Λ CDM or with standard rulers. These rankings are shown in Table 8 (with respect to Λ CDM $(-1, 0)$) and in Table 9 (with respect to standard ruler best fit (w_0^{SR}, w_1^{SR})).

The following comments can be made with respect to the results shown in Tables 8 and 9:

- The ranking sequences of dataset collections with respect to a. consistency with Λ CDM, b. consistency with standard rulers and c. internal consistency (Table 7) are practically identical. This is an interesting result in view of the fact that the three ranking criteria are independent of each other. Criteria a. and c. rank the quality of the datasets while criterion b. ranks the consistency with a given cosmological model. Thus, this coincidence may be viewed as evidence supporting the Λ CDM model since other parameter reference points would in general tend to spoil this ranking (see Table 4).
- More consistent collections (with any of the criteria) are those including the SNLS1 dataset while less consistent are those including the Gold06 dataset.
- Maximum consistency for all dataset collections with either Λ CDM or with standard rulers is achieved for a narrow range of Ω_{0m} ($\Omega_{0m} \in [0.27, 0.29]$). This is an indication of the robustness of the criteria used.

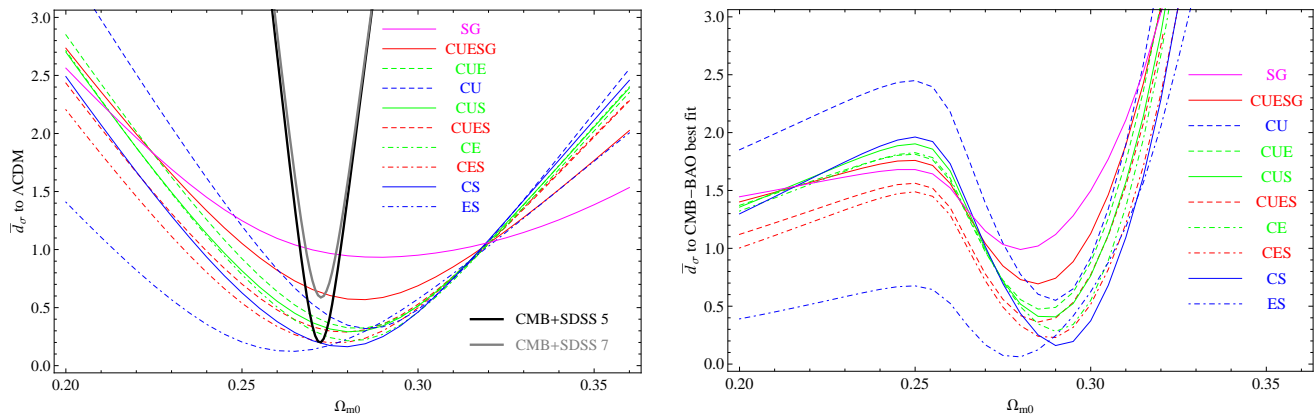


Fig. 9: a: σ -distances $\bar{d}_\sigma(\Omega_{0m}; -1, 0)$ of the Λ CDM point for the dataset collections in Table 7. The minimum values of $\bar{d}_\sigma(\Omega_{0m}; -1, 0)$ and the corresponding values of Ω_{0m} are collected in Table 8. Also shown are the σ -distances between the standard ruler best fit (SDDS5 and SDSS7) and Λ CDM (black and grey solid lines). b: σ -distances $\bar{d}_\sigma(\Omega_{0m}; (w_0, w_1)^{SR})$ to the standard ruler best fit (WMAP5+SDSS5). The minimum values of $\bar{d}_\sigma(\Omega_{0m}; (w_0, w_1)^{SR})$ and the corresponding values of Ω_{0m} are listed in Table 9.

5. CONCLUSIONS

The main conclusions of our analysis comparing the six most recent SNIa datasets in the context of the CPL parametrization may be summarized as follows:

- All datasets can be made consistent with Λ CDM and with standard rulers at a level of 95.4% (2σ) or less for certain prior values of the matter density Ω_{0m} in the range $\Omega_{0m} \in [0.25, 0.35]$.
- The Gold06 and the SDSS-II standardized with MLCS2k2 datasets have the minimum consistency with both Λ CDM and with standard rulers while SNLS1 is the most consistent dataset with both Λ CDM and standard rulers. This may be related to the fact that Gold06 is highly inhomogeneous and includes a few outliers [22] while SNLS1 is the most homogeneous dataset. These consistency features are inherited (at a reduced degree) to other datasets of Table 1 that include parts of SNLS1 (e.g. Constitution or ESSENCE) or Gold06 (i.e. Union).
- The best fit of the Gold06 dataset (and of the Union that includes part of it) corresponds to a universe that super-accelerates at present ($w(z=0) = w_0 < -1$) after having crossed the phantom divide line (PDL) $w = -1$ at a recent redshift ($w_1 > 0$) (see Fig. 3). On the other hand the best fit of the Constitution dataset gives a reversed behavior: no super-acceleration at present ($w_0 > -1$) but for $\Omega_{0m} > 0.25$ it crosses the PDL at a recent redshift leading $w(z) < -1$ in the recent past since $w_1 < 0$ (see Fig. 3). This behavior has been discussed in some detail in Ref. [39]. We stress that this is only the behavior of the best fit and should not be taken

as a statistically significant trend of the cosmic history indicated by the datasets.

- All six datasets are statistically mutually consistent. However, this consistency is somewhat reduced for dataset collections that include the Gold06 dataset (see Fig. 8 and Table 7). This is consistent with previous analyses [22] that pointed out non-uniformity systematics in the Gold06 dataset.
- The SDSS-II dataset obtained with the MLCS2k2 fitter has reduced consistency with both Λ CDM and with standard rulers in contrast with the same dataset standardized with the SALT2 fitter which appears similar with the other datasets and consistent with Λ CDM. We have verified that this is not a general deficiency of the MLCS2k2 because other datasets using the same fitter (e.g. ESSENCE or the MLCS version of the Constitution dataset) appear fairly normal and consistent (see Fig. 3). Therefore we have not been able to trace the origin of the peculiar nature of the SDSS-II MLCS2k2 dataset.

It is interesting that despite the improvement of standard ruler and standard candle data quality during the last decade the consistency of Λ CDM with data has not decreased despite the fact that Λ CDM is a simple, specific and well defined model which appears as a measure-zero point in all generalized models. On the contrary its consistency seems to be improving with time as new and more accurate data appear. For example, the Constitution SNIa dataset which is a very recent compilation with a drastic improvement on the crucial nearby SNIa sample, is also one of the most consistent datasets with both Λ CDM and standard rulers.

Despite of its excellent consistency with both SnIa standard candles and CMB-BAO standard rulers, Λ CDM has to face potential challenges from other cosmological data [25] (e.g. large scale velocity flows, galaxy and cluster halo profiles, peculiar features of CMB maps etc.) which may lead the quest for the properties of dark energy to interesting surprises in the near future. Such surprises may also come from future standard candle observations or standard ruler CMB experiments (e.g. Planck [40]) which are expected to significantly improve the accuracy of the constraints discussed in the present study.

Numerical Analysis Files: The mathematica files and datasets used for the production of the figures may be downloaded from <http://leandros.physics.uoi.gr/datacomp/>

We have tested that these files reproduce the results of the original dataset papers [5, 6, 7, 8, 9, 10] in the special case of constant w considered there.

Acknowledgements

We thank R. Kessler for useful comments. This work was supported by the European Research and Training Network MRTN-CT-2006 035863-1 (UniverseNet). S. N. also acknowledges support by the Niels Bohr International Academy and the Danish Research Council under FNU Grant No. 272-08-0285.

-
- [1] Hamuy et al. 1996, AJ, 112, 2408; Riess et al. 1999, AJ, 117, 707; Jha 2002 (PhD thesis Harvard); Krisciunas 2001, AJ, 122, 1616; Krisciunas, et al. 2004b, AJ, 128, 3034, (arXiv:astro-ph/0409036); Altavilla et al, MNRAS, **349**, 1344 (2004) [arXiv:astro-ph/0401273];
- [2] Perlmutter et al. 1999, ApJ, 517, 565; Knop et al. 2003, ApJ, 598, 102;
- [3] Riess et al. 1998 AJ, 116, 1009; Clocchiatti et al. 2003, astro-ph/0310432; Riess et al. 2000, ApJ, 536, 62; Tonry et al. 2003, Astrophys.J.594:1-24,2003.
- [4] A. G. Riess *et al.* [Supernova Search Team Collaboration], Astrophys. J. **607**, 665 (2004).
- [5] M. Hicken *et al.*, Astrophys. J. **700**, 1097 (2009) [arXiv:0901.4804 [astro-ph.CO]].
- [6] M. Kowalski *et al.*, Astrophys. J. **686**, 749 (2008) [arXiv:0804.4142 [astro-ph]].
- [7] T. M. Davis *et al.*, Astrophys. J. **666**, 716 (2007) [arXiv:astro-ph/0701510].
- [8] P. Astier *et al.* [The SNLS Collaboration], Astron. Astrophys. **447**, 31 (2006) [arXiv:astro-ph/0510447].
- [9] A. G. Riess *et al.*, Astrophys. J. **659**, 98 (2007) [arXiv:astro-ph/0611572].
- [10] R. Kessler *et al.*, arXiv:0908.4274 [astro-ph.CO].
- [11] D. N. Spergel *et al.* [WMAP Collaboration], Astrophys. J. Suppl. **170**, 377 (2007) [arXiv:astro-ph/0603449].
- [12] E. Komatsu *et al.* [WMAP Collaboration], Astrophys. J. Suppl. **180**, 330 (2009) [arXiv:0803.0547 [astro-ph]].
- [13] D. J. Eisenstein *et al.* [SDSS Collaboration], Astrophys. J. **633**, 560 (2005) [arXiv:astro-ph/0501171].
- [14] W. J. Percival, S. Cole, D. J. Eisenstein, R. C. Nichol, J. A. Peacock, A. C. Pope and A. S. Szalay, arXiv:0705.3323 [astro-ph].
- [15] W. J. Percival *et al.*, arXiv:0907.1660 [astro-ph.CO].
- [16] M. Tegmark *et al.* [SDSS Collaboration], Phys. Rev. D **69**, 103501 (2004) [arXiv:astro-ph/0310723]
- [17] H. K. Jassal, J. S. Bagla and T. Padmanabhan, Phys. Rev. D **72**, 103503 (2005) [arXiv:astro-ph/0506748]; Y. Wang and P. Mukherjee, Phys. Rev. D **76**, 103533 (2007) [arXiv:astro-ph/0703780]; M. J. Mortonson, W. Hu and D. Huterer, Phys. Rev. D **79**, 023004 (2009) [arXiv:0810.1744 [astro-ph]]; Y. Wang, Phys. Rev. D **78**, 123532 (2008) [arXiv:0809.0657 [astro-ph]]; L. Samushia and B. Ratra, arXiv:0806.2835 [astro-ph]; Y. Wang, Phys. Rev. D **77**, 123525 (2008) [arXiv:0803.4295 [astro-ph]]; S. Qi, F. Y. Wang and T. Lu, arXiv:0803.4304 [astro-ph]; C. Bogdanos and S. Nesseris, JCAP **0905**, 006 (2009) [arXiv:0903.2805 [astro-ph.CO]]; C. W. Chen, J. A. Gu and P. Chen, arXiv:0903.2423 [astro-ph.CO]; R. A. Daly, M. P. Mory, C. P. O’Dea, P. Kharb, S. Baum, E. J. Guerra and S. G. Djorgovski, Astrophys. J. **691**, 1058 (2009) [arXiv:0710.5112 [astro-ph]].
- [18] P. J. E. Peebles and B. Ratra, Rev. Mod. Phys. **75**, 559 (2003) [arXiv:astro-ph/0207347]; T. Padmanabhan, Phys. Rept. **380**, 235 (2003) [arXiv:hep-th/0212290]; S. M. Carroll, Living Rev. Rel. **4**, 1 (2001) [arXiv:astro-ph/0004075]; V. Sahni, Class. Quant. Grav. **19**, 3435 (2002) [arXiv:astro-ph/0202076].
- [19] R. Durrer and R. Maartens, arXiv:0811.4132 [astro-ph]; S. Basilakos, M. PLionis and J. Sola, arXiv:0907.4555; E. O. Kahya, V. K. Onemli and R. P. Woodard, arXiv:0904.4811 [gr-qc]; M. A. Dantas and J. S. Alcaniz, arXiv:0901.2327 [astro-ph.CO]; V. Sahni, A. Shafieloo and A. A. Starobinsky, Phys. Rev. D **78**, 103502 (2008) [arXiv:0807.3548 [astro-ph]]; M. Sami, arXiv:0904.3445 [hep-th]; S. del Campo, R. Herrera and D. Pavon, JCAP **0901**, 020 (2009) [arXiv:0812.2210 [gr-qc]]; H. K. Jassal, J. S. Bagla and T. Padmanabhan, Mon. Not. Roy. Astron. Soc. **356**, L11 (2005) [arXiv:astro-ph/0404378]; S. Dutta, E. N. Saridakis and R. J. Scherrer, Phys. Rev. D **79**, 103005 (2009) [arXiv:0903.3412 [astro-ph.CO]]; H. K. Jassal, J. S. Bagla and T. Padmanabhan, arXiv:astro-ph/0601389.
- [20] B. Boisseau, G. Esposito-Farese, D. Polarski and A. A. Starobinsky, Phys. Rev. Lett. **85**, 2236 (2000) [arXiv:gr-qc/0001066]; T. Padmanabhan, arXiv:0807.2356 [gr-qc]; E. Bertschinger, Astrophys. J. **648**, 797 (2006) [arXiv:astro-ph/0604485]; J. P. Uzan, Gen. Rel. Grav. **39**, 307 (2007) [arXiv:astro-ph/0605313]; L. Amendola, R. Gannouji, D. Polarski and S. Tsujikawa, Phys. Rev. D **75**, 083504 (2007) [arXiv:gr-qc/0612180]; L. Perivolaropoulos, JCAP **0510**, 001 (2005) [arXiv:astro-ph/0504582]; I. Thongkool, M. Sami, R. Gannouji and S. Jhingan, arXiv:0906.2460 [hep-th]; B. Jain and P. Zhang, arXiv:0709.2375 [astro-ph]; S. Nesseris and L. Perivolaropoulos, Phys. Rev. D **73**, 103511 (2006) [arXiv:astro-ph/0602053];

- S. Wang, L. Hui, M. May and Z. Haiman, Phys. Rev. D **76**, 063503 (2007) [arXiv:0705.0165 [astro-ph]]; S. Tsujikawa, Phys. Rev. D **76**, 023514 (2007) [arXiv:0705.1032 [astro-ph]]; M. Jamil, E. N. Saridakis and M. R. Setare, arXiv:0906.2847 [hep-th]; S. Nesseris and L. Perivolaropoulos, Phys. Rev. D **75**, 023517 (2007) [arXiv:astro-ph/0611238].
- [21] J. Guy et al. A&A **443**, 781 (2005); J. Guy et al., A&A **466**, 11 (2007); S. Jha, A. G. Riess and R. P. Kirshner ApJ, **659**, 122, (2007).
- [22] S. Nesseris and L. Perivolaropoulos, JCAP **0702**, 025 (2007) [arXiv:astro-ph/0612653].
- [23] H. Wei, arXiv:0906.0828 [astro-ph.CO].
- [24] W. Hu, M. Fukugita, M. Zaldarriaga and M. Tegmark, Astrophys. J. **549**, 669 (2001) [arXiv:astro-ph/0006436]; W. J. Percival *et al.* [The 2dFGRS Team Collaboration], Mon. Not. Roy. Astron. Soc. **337**, 1068 (2002) [arXiv:astro-ph/0206256].
- [25] L. Perivolaropoulos, arXiv:0811.4684 [astro-ph]; R. J. Yang and S. N. Zhang, arXiv:0905.2683 [astro-ph.CO];
- [26] A. J. Albrecht *et al.*, arXiv:astro-ph/0609591; arXiv:0901.0721
- [27] E. V. Linder, Astropart. Phys. **26**, 102 (2006) [arXiv:astro-ph/0604280].
- [28] M. Chevallier and D. Polarski, Int. J. Mod. Phys. D **10**, 213 (2001) [arXiv:gr-qc/0009008].
- [29] E. V. Linder, Phys. Rev. Lett. **90**, 091301 (2003) [arXiv:astro-ph/0208512].
- [30] L. Perivolaropoulos and A. Shafieloo, Phys. Rev. D **79**, 123502 (2009) [arXiv:0811.2802 [astro-ph]].
- [31] S. Nesseris and L. Perivolaropoulos, JCAP **0701**, 018 (2007) [arXiv:astro-ph/0610092].
- [32] R. Lazkoz, S. Nesseris and L. Perivolaropoulos, JCAP **0807**, 012 (2008) [arXiv:0712.1232 [astro-ph]].
- [33] G. Miknaitis *et al.*, Astrophys. J. **666**, 674 (2007) [arXiv:astro-ph/0701043].
- [34] S. Jha, A. G. Riess and R. P. Kirshner, Astrophys. J. **659** (2007) 122.
- [35] W. M. Wood-Vasey *et al.* [ESSENCE Collaboration], Astrophys. J. **666** (2007) 694.
- [36] S. Nesseris and L. Perivolaropoulos, Phys. Rev. D **72**, 123519 (2005) [arXiv:astro-ph/0511040].
- [37] S. Nesseris and L. Perivolaropoulos, Phys. Rev. D **70**, 043531 (2004) [arXiv:astro-ph/0401556].
- [38] W. H. Press *et al.*, "Numerical Recipes", Cambridge University Press (1994).
- [39] A. Shafieloo, V. Sahni and A. A. Starobinsky, arXiv:0903.5141 [astro-ph.CO].
- [40] Planck Collaboration, The Science Programme of Planck [arXiv:astro-ph/0604069].